UC San Diego
UC San Diego Previously Published Works

Title

Laminin targeting of a peripheral nerve-highlighting peptide enables degenerated nerve visualization.

Permalink

https://escholarship.org/uc/item/6k0191rj

Journal

Proceedings of the National Academy of Sciences of the United States of America, 113(45)

ISSN

0027-8424

Authors

Glasgow, Heather L
Whitney, Michael A
Gross, Larry A
et al.

Publication Date

2016-11-01

DOI

10.1073/pnas.1611642113

Peer reviewed

Laminin targeting of a peripheral nerve-highlighting peptide enables degenerated nerve visualization

Heather L. Glasgow[a,1], Michael A. Whitney[a], Larry A. Gross[b], Beth Friedman[a], Stephen R. Adams[a], Jessica L. Crisp[b], Timon Hussain[c], Andreas P. Frei[d], Karel Novy[d], Bernd Wollscheid[d], Quyen T. Nguyen[c], and Roger Y. Tsien[a,b,e,2]

[a]Department of Pharmacology, University of California, San Diego, La Jolla, CA 92093; [b]Howard Hughes Medical Institute, University of California, San Diego, La Jolla, CA 92093; [c]Division of Otolaryngology–Head and Neck Surgery, University of California, San Diego, La Jolla, CA 92093; [d]Institute of Molecular Systems Biology at the Department of Health Sciences and Technology, CH-8093 Zurich, Switzerland; and [e]Department of Chemistry and Biochemistry, University of California, San Diego, La Jolla, CA 92093

Target-blind activity-based screening of molecular libraries is often used to develop first-generation compounds, but subsequent target identification is rate-limiting to developing improved agents with higher specific affinity and lower off-target binding. A fluorescently labeled nerve-binding peptide, NP41, selected by phage display, highlights peripheral nerves in vivo. Nerve highlighting has the potential to improve surgical outcomes by facilitating intraoperative nerve identification, reducing accidental nerve transection, and facilitating repair of damaged nerves. To enable screening of molecular target-specific molecules for higher nerve contrast and to identify potential toxicities, NP41's binding target was sought. Laminin-421 and -211 were identified by proximity-based labeling using singlet oxygen and by an adapted version of TRICEPS-based ligand-receptor capture to identify glycoprotein receptors via ligand cross-linking. In proximity labeling, photooxidation of a ligand-conjugated singlet oxygen generator is coupled to chemical labeling of locally oxidized residues. Photooxidation of methylene blue–NP41-bound nerves, followed by biotin hydrazide labeling and purification, resulted in light-induced enrichment of laminin subunits $\alpha4$ and $\alpha2$, nidogen 1, and decorin (FDR-adjusted P value $< 10^{-7}$) and minor enrichment of laminin-$\gamma1$ and collagens I and VI. Glycoprotein receptor capture also identified laminin-$\alpha4$ and -$\gamma1$. Laminins colocalized with NP41 within nerve sheath, particularly perineurium, where laminin-421 is predominant. Binding assays with phage expressing NP41 confirmed binding to purified laminin-421, laminin-211, and laminin-$\alpha4$. Affinity for these extracellular matrix proteins explains the striking ability of NP41 to highlight degenerated nerve "ghosts" months posttransection that are invisible to the unaided eye but retain hollow laminin-rich tubular structures.

nerve highlighting | laminin | proximity-based labeling | molecular imaging | surgery with molecular navigation

Molecular interactions including ligand–receptor binding are a key component of nearly every biological process. Discovering such interactions is especially challenging if they are low affinity, context-dependent, or the receptors are difficult to isolate. However, their identification improves our fundamental understanding of biological processes and enables development of synthetic ligands with clinical applications. Phage display is a powerful affinity-based molecular selection tool that has enabled the generation of peptides, proteins, and antibodies that bind to specific targets (1). Selections against complex sources, such as live cells, cell extracts, or organs, have also yielded promising results (2–4). Despite the obvious implications of these ligands as potential clinical agents and their receptors as biomarkers, few targets have been defined (5).

A variety of methods to capture native ligand–receptor interactions have used chemical or photo–cross-linking followed by mass spectrometry (MS), some requiring that ligands retain binding activity after potentially disruptive chemical treatment (6–9). In most cross-linking techniques, the ligand must reach an appropriately reactive site on the target for cross-linking to occur, while being conjugated to a potentially bulky purification tag, which can weaken specific binding. Proximity-based labeling techniques using fusion proteins have recently been

developed for the discovery of new interacting or nearby proteins (10–12); however, bulky fusion proteins are likely to affect ligand binding.

To more efficiently capture low-affinity and easily disrupted interactions, a small molecule proximity tagging method was developed using photooxidation coupled to affinity tagging (Fig. 1). A light-driven, singlet oxygen-generating molecule [SOG; e.g., methylene blue (MB), fluorescein derivative] is conjugated to a ligand. Upon binding of the ligand–SOG to tissue and exposure to light, oxidation of molecules proximal to the ligand occurs. In biological samples, singlet oxygen has an extremely short half-life, in the range of hundredths to tenths of a microsecond, during which it is estimated to diffuse within a range of tens of nanometers from its source (13, 14). Proteins are a major biological quencher of singlet oxygen, and reaction with specific amino acids forms byproducts containing ketones and aldehydes (15, 16). Such carbonyl groups are normally rare in tissues, enabling site-specific labeling of oxidized amino acids on proximal proteins. For example, tryptophan is converted into ketone-containing kynurenine or N-formylkynurenine (17–19). Biotin-conjugated hydrazides or hydrazines (BHs) have specific reactivity for ketones and aldehydes (15, 20). BHs can be reacted with tissue exogenously (Fig. 1, scheme A) or coupled directly to the ligand–SOG (Fig. 1, scheme B), allowing photooxidation and chemical conjugation to be performed simultaneously in vivo. Biotin-tagged proteins are then purified from tissue homogenates with immobilized

Significance

A fluorescently labeled nerve-binding peptide, NP41, holds promise to reduce surgical nerve damage and facilitate nerve repair. Clinical translation hinges on identification of binding targets to assess potential toxicity and understand the mechanism. For target identification, we developed a receptor capture method, enabling covalent tagging and identification of proteins within close proximity to a bound ligand. Extracellular matrix proteins laminin-421 and -211 were identified as NP41 binding targets, and TRICEPS-based glycoprotein capture supported laminin-421 as the primary binding target. This result explains the ability of NP41 to highlight degenerated nerve "ghosts" months after transection that were invisible to the unaided eye but contain laminins. Targeting extracellular matrix is advantageous for clinical imaging agents, likely reducing undesirable neurological effects.
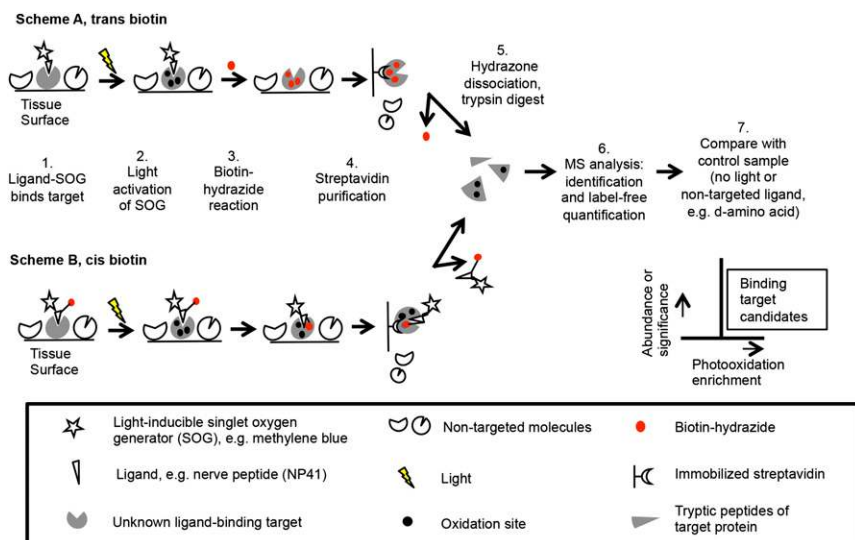
Fig. 1. Schematic of photooxidation-mediated identification of ligand-proximal molecules. (*Scheme A*) A ligand of interest is conjugated to a SOG and applied to tissue with ligand-binding activity. Upon excitation with SOG-activating light, singlet oxygen is produced, which reacts locally and results in oxidation sites, including ketones and aldehydes. BH is applied to label these carbonyl groups. Biotinylated proteins are streptavidin-purified from tissue homogenate. The hydrazone bond is released, and proteins are trypsinized and analyzed by LC–MS/MS. Label-free quantification is used to compare relative protein amounts to a control sample using NL or a nontargeted ligand such as the D-enantiomer. (*Scheme B*) Ligand is conjugated to SOG, biotin, and a ketone-reactive group—for example, pyridylhydrazine—and treated on ligand-binding tissue. Tissue is exposed to light, and biotinylated proteins are purified and identified as before.

streptavidin, dissociated via acidic hydrolysis of the hydrazone bond (21), digested with trypsin, and identified by liquid chromatography-tandem mass spectrometry (LC–MS/MS). Label-free quantification is then used to compare protein abundance relative to a control.

Alternatively, ligand-directed receptor capture (LRC) using TRICEPS technology has been shown to enable carbohydrate-directed tagging of receptors and subsequent identification by MS (8, 9). Mild sodium periodate ($NaIO_4$) treatment oxidizes cis-glycol groups in carbohydrates to aldehydes, and newly generated aldehydes cross-link to a BH-containing ligand. Samples are then purified using immobilized streptavidin and released by the endoglycosidase PNGaseF.

In this report, ligand-proximal photooxidation and an adapted version of TRICEPS LRC of glycoproteins were used to identify extracellular matrix proteins laminin-421 and -211 as the binding targets of NP41. This nerve-binding peptide was previously identified by phage display and shown to fluorescently label nerves in vivo and improve surgical identification, potentially reducing iatrogenic nerve injury (2, 22, 23). This result explains NP41's striking ability to highlight otherwise invisible, highly degenerated nerves, which are devoid of myelin and axons but contain laminin-rich extracellular matrix.

Results

To identify NP41 binding targets, affinity chromatography was chosen as the initial method of isolation. Homogenized nerve was passed over immobilized NP41 versus the control D-amino acid enantiomer, which was previously found not to bind nerves when injected into mice (2). No specific protein was selectively captured as determined by MS analysis, leading us to speculate that NP41 bound with low affinity to homogenates. Thus, to capture NP41-receptor interaction in situ, we developed a method for proximity labeling ligand-bound proteins using photooxidation and targeted BH labeling and also tested previously described glycoprotein capture using TRICEPS-based chemistry (8, 9).

To test the concept of proximity-based oxidation of proteins through photoactivation of a ligand–SOG conjugate, ketone adducts were directly measured via MS following light exposure. Specifically, biotin–MB, used as a ligand–SOG, and streptavidin were coincubated, and then MB was photoactivated with 615/40 nm light for 0–90 s. Streptavidin was digested with trypsin and subjected to LC–MS/MS. MS1-based label-free quantification showed a light and ligand–MB-dependent increase in tryptophan oxidation in streptavidin peptides with +4 (kynurenine) and +16 (tryptophan–OH) mass changes (Fig. S1 *A–C*). Peak conversion occurred after brief light exposures (30 s and 3 s, respectively) with

relatively lower conversion after longer exposures. This may be due to compounding reactions by singlet oxygen that result in diverse or unidentifiable products, many of which are unstable (16).

Imaging Biotinylation upon Ligand-Proximal Photooxidation. To examine whether photoactivation of a NP41–SOG conjugate would result in spatially localized BH labeling proximal to the binding site, mouse peripheral nerve sections were incubated with carboxyfluorescein (FAM)-labeled NP41 and photooxidized with 480 nm light. Controls including D-enantiomer and no light (NL) treatment were done in parallel. Oxidized sites were labeled with 50 μM BH in MES buffer, pH 5.5, and stained with streptavidin–Texas Red. High biotin staining was detected at the perineurium upon photooxidation with NP41–FAM, which correlated well with peptide binding as detected by fluorescence (Fig. 2). Neither the D-enantiomer control nor non–light-exposed tissues showed high perineurial labeling, and photobleaching of FAM occurred in the photooxidized (PO) sample, consistent with singlet oxygen destruction of the fluorophore.

Proximal Photooxidation and BH Labeling Identify Laminin-α4, Laminin-α2, and Nidogen as Candidate NP41 Binding Targets. Experiments to identify NP41 binding partners by proximal photooxidation and MS were done both ex vivo on intact excised nerves and in vivo by injecting the probe into mice. For ex vivo experiments, NP41–MB (Fig. 3, *Top*) was used to enhance distribution of photooxidation throughout the nerve. MB has superior singlet oxygen production, and red light (640 nm) penetrates deeper into tissue than 488 nm (fluorescein excitation) light. Intact mouse sciatic nerves were treated with 50 μM NP41–MB for 2 h, rinsed, and photooxidized with 640 nm light for 10 s, 1 min, or 15 min or not exposed to light as a control (t = 0). Nerves were reacted with 50 μM BH and homogenized. Proteins were affinity-purified on avidin beads, released by acid hydrolysis, trypsinized, and identified by LC–MS/MS. Protein enrichment of PO samples compared with the NL control was determined as the fraction of the average spectral counts in PO samples relative to total spectral counts (PO/PO + NL).

A select group of proteins including several laminins were enriched over the NL control (PO/PO + NL > 0.5) when spectral counts of different light-exposed samples were averaged or compared individually (Fig. S2). Proteins with abundant counts (>30) that showed the highest enrichment were laminin subunits α4 and β2 (0.76 and 0.72, average), which were enriched after only 10 s of photooxidation (0.79 and 0.72, at 10 s). Laminin subunits β1 (0.65, average), γ1 (0.57), and α2 (0.56); nidogen (0.64); and collagen VI chains α1, α2, and α3 (0.56, 0.57, and 0.55, respectively) were also

Fig. 2. Ligand-proximal photooxidation results in specific biotinylation of regions highlighted by NP41. Photooxidation of NP41–FAM-treated nerve tissue sections with 480/30 nm light induces BH labeling detected with streptavidin–Texas Red (red, *Left* panels), which is highest in the perineurium (white arrows) that ensheathes the myelinated Schwann cell–axon bundles. High perineurial biotin labeling is absent from both the NP41–FAM NL control and from all D-NP41 controls, both with and without photooxidation. Perineurial biotin labeling colocalizes with direct detection of peptide binding at the perineurium in the same section (green, *Right* panels). Perineurium was confirmed in all sections by plane light microscopy and autofluorescence when images were scaled to maximum gain. Images are at matched gain within each color and representative of at least three independent samples. (Scale bar, 50 μm.)

enriched, and spectral counts were greatest after 15 min of photooxidation. Other highly abundant peripheral nerve-specific proteins, such as neurofilament light chain (0.41) and myelin protein P0 (0.41), showed no enrichment under light-exposed conditions. To normalize signal within each sample and test for significance, precursor ion abundance was used as an alternate measure of quantifying protein enrichment in light-exposed versus non–light-exposed samples. The most statistically significant enriched proteins after 15 min of light exposure were laminin-α4, -α2, and nidogen-1 (Fig. 3, *Bottom*; log2FC = 5.09, 3.06, and 2.83, respectively; adj. *P* value < 10^{-7}). Decorin was also identified as significantly enriched (log2FC = 8.38; adj. *P* value < 10^{-7}); however, it was not enriched by spectral count quantitation. Laminin-γ1 and collagen VI and I chains were among other proteins enriched with higher *P* values, whereas laminin β1 and β2 chains showed enrichment below the significance cutoff.

To confirm NP41's potential interaction with these proteins in vivo, a SOG and pyridylhydrazine–biotin (HB) were directly conjugated to NP41 (Fig. 1, scheme B). Dibromofluorescein (DBF) was used as the singlet oxygen generator due to its efficient production of singlet oxygen compared with fluorescein and because it showed greater compatibility with NP41 targeting in vivo compared with MB (Fig. S3). DBF–NP41–HB (Fig. S4A) or its D-enantiomer control was injected into mice. Four hours postinjection, sciatic nerves on one side were surgically uncovered and photooxidized with 480 nm light (PO), whereas the contralateral side was kept in the dark (NL). Both sciatic nerves were dissected, immersed in MES buffer pH 5.5, and processed as previously described. Spectral counting of the PO versus the NL control revealed enrichment of nidogen-1 and -2 (1 and 0.8); laminin subunits α4 (1.0), β2 (0.78), γ1 (0.88), α2 (0.83), and β1 (0.67); heparan sulfate proteoglycan (Hspg, 0.78); and slight enrichment of collagen VI α1 (0.67), α2 (0.61), and α3 (0.61), (Fig. S4 *B and C*). The D-enantiomer control showed poor enrichment and lower spectral counts (Fig. S4D). An additional laminin subunit, α5, was identified as enriched with very few low spectral counts. Other enriched proteins either had ratios similar to the D-enantiomer control or showed low or no abundance in the previous MB–NP41 photooxidation experiment (Fig. S4E).

Identification of Laminin-α4 and -γ1 as Candidate NP41 Targets by TRICEPS-Based Ligand-Directed Glycoprotein Cross-Linking.

Because laminins and other extracellular matrix proteins are heavily glycosylated (24), a modified TRICEPS-based (8) procedure was used to capture in vivo targets of NP41. NP41–fluorescein–biotin hydrazine (NP41–FAM–HB; Fig. 4, *Right*) was first injected into mice, and excised nerves were treated with periodate to cross-link prebound peptide. Histological imaging of nerves labeled by systemic injection of NP41–FAM–HB showed similar localization to NP41–FAM (Fig. S5A). High retention of fluorescence was apparent in periodate-treated nerves and not in control-treated nerves, demonstrating hydrazine-mediated cross-linking (Fig. S5B).

For target identification, NP41–FAM–HB or a D-enantiomer control was injected into mice, and nerves were excised before periodate application, then processed and analyzed as previously described (8). Quantification of individual peptides containing formerly glycosylated asparagine residues (N[115]-X-S/T motif) revealed laminin-γ1 and -α4 as enriched in the NP41-treated sample over the control (Fig. 4, *Left*). Specifically enriched peptides included laminin-γ1 peptides TAN[115]ETSAEAYNLLLR, RIPAIN[115]R, and IASAVQKN[115]ATSTKADAER and laminin-α4 peptide HVTDMN[115]STIHLLR.

Confirmation of Ligand–Target Colocalization and NP41–Laminin Binding.

Laminins are trimers of α, β, and γ subunits that complex with nidogen, collagen IV, and Hspg to form basement membranes (25). Collagen VI is a trimer of α1–3 chains and forms microfibrils, collagen I forms fibrils, and decorin is a small proteoglycan that bridges the two (26, 27). Laminin-α4β2γ1 (laminin-421), laminin-α5β2γ1 (laminin-521), laminin-α2β1γ1 (laminin-211), and collagen VI have been previously shown to localize in the peripheral nerve (28, 29).

Fig. 3. Ligand-proximal photooxidation of NP41–MB identifies binding candidates laminin, collagen, and associated proteins. (*Top*) Structure of NP41-MB conjugate. MB causes photooxidation at 650 nm. (*Bottom*) Comparison of protein abundance in the PO sample versus NL control. Shown is the label-free quantitation using relative precursor ion signal and significance testing of the PO sample (15 min) versus NL control. The most significantly enriched proteins include laminin subunits α4 (Lama4) and α2 (Lama2), nidogen 1 (Nid1), and decorin (Dcn). Proteins with less significant enrichment (*P* < 0.01) include collagen VI chains (Col6a1, Col6a2) and laminin-γ1 (Lamc1). Laminin-β1 (Lamb1) and -β2 (Lamb2) were not significantly enriched.

To directly compare the histological localization of NP41 in vitro and in vivo with candidate binding targets in nerve, FAM- or Cy5-conjugated NP41 was topically applied to mouse facial nerve sections or injected into mice before dissection and imaging. Perineurial staining was striking both in vitro (topically applied) and in vivo (systemically injected), whereas endoneurial basement membrane labeling was more prevalent in in vivo- than in in vitro-labeled nerves (Fig. 5A). For comparison, analogous mouse facial nerve sections were treated with antibodies to laminin-α4, -α5, -α2, -β2, and -γ1 and collagen VI α1 and α3 and fluorescent secondary antibody. Although laminin-α5 did not show abundant enrichment by ligand-proximal photooxidation and was not identified by glycoprotein capture, it is known to form a complex with laminin subunits β2 and γ1 in sciatic nerves, making it a candidate of interest (28). Anti–laminin-α4 and -α5 showed mostly perineurial staining, whereas anti–laminin-α2 labeled only endoneurial basement membranes, and anti–laminin-β2 and -γ1 and collagen VI chains highlighted both the perineurium and endoneurium (Fig. 5B). Nidogen and Hspg, also identified as enriched by ligand-proximal photooxidation, are ubiquitously expressed basement membrane proteins known to complex with most laminin isoforms (25) and may be photooxidized due to their proximity to the nerve-specific target or pulled down in complex with laminins.

To test NP41–laminin binding, multivalent NP41-expressing M13 phage, from which NP41 was originally discovered (2), or control phage expressing a library of random peptides (X12) was added to plates coated with purified recombinant protein; laminin-421, -521, and -211; or collagen VI and detected with an anti-M13 antibody labeled with horseradish peroxidase. NP41–phage showed significantly greater binding than X12-phage to laminin-421 and -211 ($P < 0.01$, Student's t test) but not to collagen VI ($P = 0.07$) or laminin-521 ($P = 0.25$; Fig. 5C), neither of which showed great enrichment with the MS techniques. This led us to believe that binding occurred through the α4 domain. To control for the possibility that purified laminins contained nidogen, which was identified in photooxidation experiments but not in carbohydrate-directed LRC and could be the source of NP41 affinity, the assay was repeated on plates coated with laminin-α4, nidogen-1, or nidogen-2. NP41–phage showed significantly higher binding to purified laminin-α4 subunit than did X12 control phage ($P < 0.01$) and no binding to either nidogen-1 or -2 (Fig. S6).

Confirmation of Laminin Colocalization with NP41 in Nerve Degeneration Model. Following nerve injury and subsequent Wallerian degeneration, the tubular space previously occupied by the axon within the nerve becomes infiltrated with immune cells. Many components are cleared, such as myelin and neurofilament, however the extracellular matrix structure and component proteins are retained or up-regulated (30, 31). Because NP41 showed evidence of binding

to structural targets, NP41 colocalization with laminin expression was examined in a degenerated nerve model (22, 23). NP41–FAM was injected into mice in which the main branch of the facial nerve had been surgically transected 3 mo prior and allowed to degenerate. Consistent with NP41 binding of extracellular matrix, fluorescence imaging showed NP41–FAM labeling of degenerated nerves in vivo that were not detectable by white light reflectance (Fig. 6A). To verify NP41 binding histologically, cryosections of degenerated facial nerve within surrounding tissues at 6 wk and 2.5 mo posttransection were treated with NP41–FAM, stained with hematoxylin and eosin (H&E), or immunostained for subunits of laminin-421 and -211. In sections, NP41 labeling showed consistent perineurial staining in highly cellular, demyelinated nerves (Fig. 6B). Immunostaining similarly revealed the retention of laminin-421 and -211, which colocalized at the perineurium and endoneurial basement membranes (Fig. 6C).

Discussion

Fluorescent highlighting of peripheral nerves with molecules like NP41-dye conjugates offers the potential to improve a myriad of surgical procedures by reducing morbidity caused by inadvertent nerve injury. However, characterization of the molecular basis of nerve targeting, which hinges on the identification of the binding target, is necessary for clinical translation. Optimization of NP41 binding to laminins may result in improved peptides, thus facilitating enhanced nerve visualization and repair and preventing nerve damage. Toward this goal, laminin-421 and -211 have here been identified as likely binding targets of NP41 using a ligand-proximal photooxidation assay. An adapted version of previously reported TRICEPS-based LRC also identified laminin-421 chains, suggesting that it is a principle target in vivo. This conclusion was supported by prominent perineurial colocalization of NP41 and laminin subunits α4, β2, and γ1 in healthy and degenerated nerve. The ability of phage displaying NP41 peptide to bind purified laminin-421 as well as laminin-211 supported interaction with both proteins. We speculate that targeting is primarily mediated through α4 subunit as evidenced by striking staining of the perineurium, significant NP41 binding to laminin-421 and α4 laminin subunit, and the lack of significant binding to laminin-521.

Laminins and collagens form extracellular matrix in the majority of tissues but are diverse in their composition of subunit isoforms. Although laminin-421 has tissue-selective expression, it is not neural-exclusive, as it is expressed in other tissues including blood vessels (28). Having been developed by phage display selection for binding intact nerves, it is logical that NP41 targets extracellular matrix and perineurial laminin given their high abundance, prominent exterior location, and the likely low tissue penetration of large phage particles (between 100 and 1,000 nm long). Targeting extracellular matrix proteins is likely beneficial for clinical imaging agents due to the high
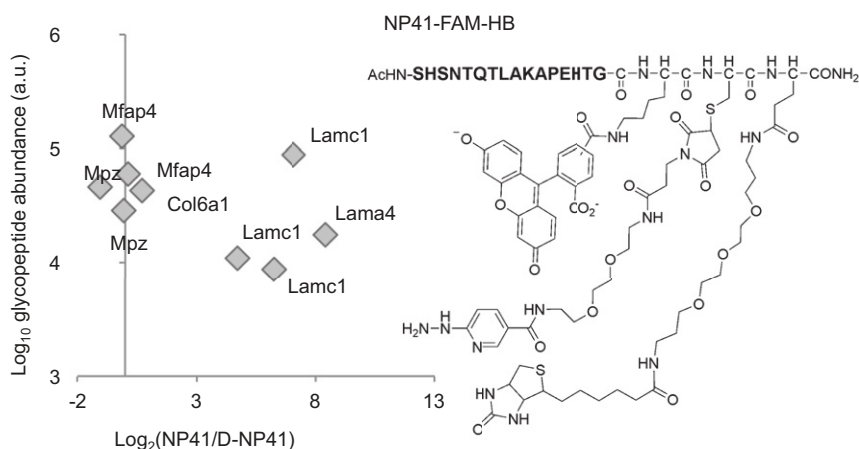
Fig. 4. Ligand-based glycoprotein receptor capture identifies laminin subunits α4 and γ1 as NP41 binding partner candidates. (*Right*) Structure of NP41–FAM–HB conjugate. Fluorescein allows for visualization of the peptide, pyridylhydrazine cross-links the peptide to glycans after tissue is oxidized with sodium periodate, and biotin is used to isolate the peptide target from nerve homogenates. (*Left*) Glycoprotein receptor capture with NP41–FAM–HB versus all D-amino acid control conjugate identifies formerly glycosylated peptides laminin-γ1 (Lamc1) and -α4 (Lama4) peptides.
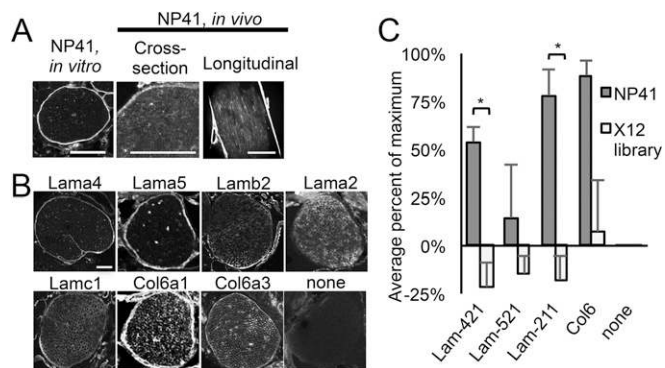
Fig. 5. NP41 colocalizes with neural laminins and collagen and binds to purified laminin-421 and -211. (*A*) NP41–FAM treated on facial nerve sections showed typical bright perineurial staining with little endoneurial staining (*Left*), whereas systemically injected NP41, imaged in sciatic nerves in cross-section (NP41-FAM, *Middle*) and longitudinally (NP41-Cy5, *Right*), shows both high perineurial staining and endoneurial basement membrane. (Scale bar, 500 μm; *Left* scale bar, 100 μm.) (*B*) Immunofluorescence of laminin and collagen subunits on mouse facial nerve tissue sections has similar localization to NP41 binding. Perineurium and endoneurial basement membranes were stained by antibodies to laminin and collagen chains. Background staining of no primary antibody control (none) was negligible. (*C*) ELISA of NP41-expressing phage shows significantly greater binding to purified laminin (Lam)-421 and -211 than control phage expressing a library of random 12-amino acid peptides (X12) but not to Lam-521 or collagen VI (Col6). Shown is the average signal of four independent experiments each performed in triplicate. Values were background-subtracted for binding to control uncoated wells and expressed as a percent of the maximum signal in each experiment. Error bars represent SEM. *P value < 0.01. Student's t test, P value = 0.0039 (Lam-421), 0.25 (Lam-521), 0.0026 (Lam-211), and 0.071 (Col6).

accessibility of these proteins from circulation and because adverse side effects may be less likely than for molecules that bind proteins within nerve axons or myelin sheaths and potentially alter nerve conduction. NP41 has been criticized for highlighting degenerated as well as live nerves (32), but we regard this as an advantage because it aids surgical repair of degenerated nerves (22, 23), whereas motor nerve function is amenable to assessment by other means.

Proximity-based labeling offers advantages over alternative approaches for fairly weak interactions because it does not necessitate retention of ligand binding during chemical treatment. Most current cross-linking methods require a specific reactive group to exist in a ligand-accessible location on the target macromolecule. This limitation is eliminated with proximal photooxidation and exogenously added BH, in which labeling potentially includes both direct ligand-binding targets as well as closely interacting proteins. In cis-labeling, hydrazine reaction is spatially limited by its tether length to the ligand, likely resulting in tagging of the closest reactive site, presumably within the direct binding target. In addition, photo–cross-linkers such as azides and diazirines are limited to UV wavelengths and can only be photolyzed once (7), whereas photooxidation is compatible with a multitude of SOGs, ranging from UV to infrared, and can undergo multiple cycles, limited only by bleaching. Disadvantages include the limited knowledge of SOG hydrazide-reactive modifications on amino acids, glycans, and lipids and potential loss of specificity due to singlet oxygen's diffusion range.

Other proximity labeling techniques for MS, such as ascorbate peroxidase coupled to biotin–phenol labeling (APEX) and promiscuous biotin ligase (BioID), use bulky enzyme conjugates requiring biological expression rather than chemical conjugation (10, 11). For the identification of intracellular interactions by photooxidation and BH labeling, genetically encodable SOGs could be substituted, such as miniSOG, FlAsH, or ReAsH (33, 34). MiniSOG's use in proximity labeling for mass spectrometry-based identification of interacting partners has

been explored using biotin-thiol to form disulfide bonds with cysteine residues on nearby proteins in the presence of singlet oxygen (12). MiniSOG was also recently demonstrated to facilitate the measurement of distances of proteins within complexes in live cells by singlet oxygen triplet energy transfer of a fluorescent singlet oxygen detector on two putative interacting proteins (35). Furthermore, ligand-proximal photooxidation techniques may be modifiable with alternatives to BH such as antibody pull-down of proteins containing methionine sulfoxide or *N*-formylkynurenine (36, 37). Future studies will address if molecules with higher affinity toward human laminin subunits α4, α5, or α2 can generate greater clinically useful nerve contrast. Alternatively, natural biomolecules known to target laminins, for instance ML-LBP21 or phenolic glycolipid (PGL-1), of the peripheral nerve-homing pathogen *Mycobacterium leprae* (38, 39) could be tested.

Materials and Methods

All experiments on mice were performed under protocols approved by the University of California, San Diego Institutional Animal Care and Use Committee. SKH1 mice (Charles River Laboratories) or wild-type albino C57BL6 mice (Jackson Laboratories) were used for all tissues. Synthesis and chemical conjugation of peptides and synthesis of DBF are described in *SI Materials and Methods*.

Ligand-Proximal Photooxidation on Tissue Sections for Imaging. Facial nerve and surrounding muscle and fasciae were embedded in Optimal Cutting Temperature (OCT) and frozen on dry ice. Sections 10 μm thick were cut on a
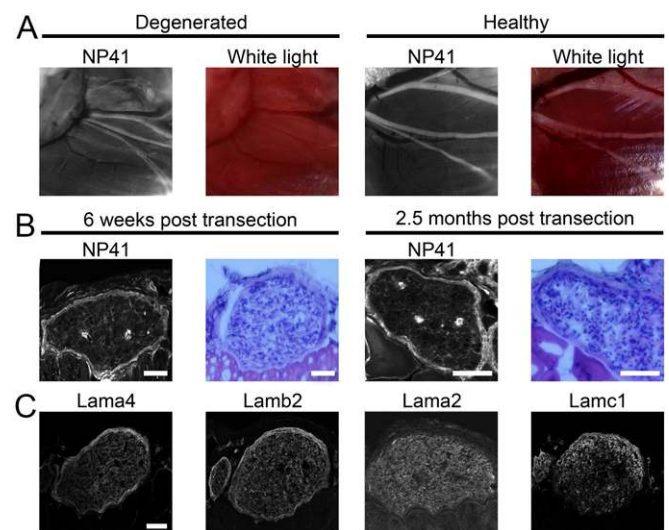

Fig. 6. Nerve peptide highlights chronically degenerated nerve ghosts due to conserved laminin structure. (*A*) NP41-FAM labeling in vivo visualized by fluorescence is retained in degenerated facial nerve (*Left*), which is invisible by white light reflectance (*Middle Left*), whereas healthy facial nerve (*Middle Right*) shows both NP41-FAM fluorescence and is visible by white light imaging (*Right*) due to the white appearance of intact myelinated nerve bundle. (*B*) NP41 staining on sections of degenerated nerve shows continued peptide binding despite extensive Wallerian degeneration. Sections of degenerated facial nerve 6 wk (*Left* and *Middle Left*) and 2.5 mo posttransection (*Middle Right* and *Right*) treated with NP41–FAM (*Left* and *Middle Right*) retain perineurial fluorescence. H&E staining (*Middle Left* and *Right*) shows that transected nerves are highly cellular (dark blue) with few myelinated sheaths (pink round structures), indicating extensive degeneration. Gain is set individually. (Scale bar, 500 μm.) (*C*) Immunostaining of laminin subunits shows retention in degenerated nerve basement membranes similar to NP41. Immunostaining on serial sections of mouse facial nerves, 6 wk posttransection, shows continued perineurial and endoneurial basement membrane staining of laminin-α4 (Lama4), laminin-β2 (Lamb2), laminin-α2 (Lama2), and laminin-γ1 (Lamc1). Gain is set individually. (Scale bar, 500 μm for all images.)

cryostat (Leica) and dried on glass slides. Tissues were preblocked with 50 μM nicotinic hydrazide in MES buffer, pH 5.5, for 30 min. NP41–FAM at 375 μM or D-amino acid control in 0.5× Hank's Buffered Saline Solution (HBSS) was added for 20 min. Slides were washed in PBS for at least 5 min and then exposed for 15 min to 480 nm excitation light (30 nm bandwidth, 0.07 W/cm^2) on a solar simulator, wheras control slides were kept dark. Slides were stained with streptavidin–Texas Red for 1 h, washed in PBS, and imaged on a confocal microscope (Zeiss) with 488 nm excitation and 505 nm LP emission (<1 s exposure) to image FAM–peptide and 532 nm excitation and 560–675 nm emission to image Texas Red. Zeiss Zen and Adobe Photoshop software were used to make composite tiled images.

Ligand-Proximal Photooxidation with NP41-MB on Whole Nerves and LC–MS/MS. Sciatic nerves were submerged in 50 μM NP41–MB in PBS for 2 h. After washing in PBS, nerves were exposed to 640 nm light for 10 s, 1 min, or 15 min or kept dark as a control. Nerves were transferred to 50 mM MES buffer, pH 5.5, with 50 μM BH for 30 min and then homogenized in PBS using a motorized tissue grinder. Sample preparation, LC–MS/MS, and data analysis are described in *SI Materials and Methods*.

TRICEPS-Based NP41–FAM–HB LRC for MS. Mice were injected with 200 nmol of FAM–NP41–HB or its D-enantiomer control into the tail vein, and four sciatic nerves each were dissected after 1.5 h. Nerves were minced and resuspended in 0.8 mL 50 mM ammonium bicarbonate (Sigma-Aldrich). Sample preparation, LC–MS/MS, and data analysis are described in *SI Materials and Methods*.

Immunofluorescence. Histological imaging of NP41 in vivo binding was performed as previously described (2). Immunostaining was performed with rabbit antisera to mouse laminin-α4, -β2, and -γ1 (kindly provided by T. Sasaki, Oita University, Oita, Japan), -α5 (kindly provided by J. Miner, Washington University, St. Louis), and collagen VI α1 and α3 and rat

antibody to laminin-α2 (clone 4H8-2, Santa Cruz Biotechnology). Additional information is provided in *SI Materials and Methods*.

Phage Binding ELISA. Plates (96-well) were coated with purified recombinant human laminin-421, -211, and -521 (Biolamina); collagen VI (Abcam); or no protein as a control at 10 μg/mL in sodium bicarbonate (7.5%), pH 9.5, at 4 °C overnight and then blocked with BSA. M13 phage expressing NP41 or random 12-amino acid peptides on pIII (Ph.D.12, New England Biolabs) were added for 1 h, washed in PBS, detected by anti-M13–HRP (GE Healthcare) and TMB 1-Step Ultra colorimetric substrate (Thermo Fisher), and measured on a Tecan plate reader at 650 nm.

Imaging NP41 of Healthy and Degenerated Nerves in Vivo. Facial nerves were transected as previously described (23). Three months after main branch transection, distal facial nerve branches were imaged, as was a healthy facial nerve control, in 6-mo-old female SKH1 mice. Mice were anesthetized with an i.p. injection of ketamine (150 mg/kg) and xylazine (10 mg/kg). We injected 20 nmol/g FAM–NP41 through the tail vein, and facial nerves were exposed and imaged after 2.5 h washout using a customized Olympus fluorescence dissecting microscope with white light reflectance and with fluorescence light with 450–490 nm excitation and 500–550 nm emission.

1. Smith GP, Petrenko VA (1997) Phage display. *Chem Rev* 97(2):391–410.
2. Whitney MA, et al. (2011) Fluorescent peptides highlight peripheral nerves during surgery in mice. *Nat Biotechnol* 29(4):352–356.
3. Pasqualini R, Ruoslahti E (1996) Organ targeting in vivo using phage display peptide libraries. *Nature* 380(6572):364–366.
4. Brown KC (2000) New approaches for cell-specific targeting: Identification of cell-selective peptides from combinatorial libraries. *Curr Opin Chem Biol* 4(1):16–21.
5. Weissleder R (2010) *Molecular Imaging: Principles and Practice* (People's Medical Pub. House–USA, Shelton, CT), p xxii, 135.
6. Sinz A (2010) Investigation of protein-protein interactions in living cells by chemical crosslinking and mass spectrometry. *Anal Bioanal Chem* 397(8):3433–3440.
7. Tanaka Y, Bond MR, Kohler JJ (2008) Photocrosslinkers illuminate interactions in living cells. *Mol Biosyst* 4(6):473–480.
8. Frei AP, et al. (2012) Direct identification of ligand-receptor interactions on living cells and tissues. *Nat Biotechnol* 30(10):997–1001.
9. Frei AP, Moest H, Novy K, Wollscheid B (2013) Ligand-based receptor identification on living cells and tissues using TRICEPS. *Nat Protoc* 8(7):1321–1336.
10. Rhee HW, et al. (2013) Proteomic mapping of mitochondria in living cells via spatially restricted enzymatic tagging. *Science* 339(6125):1328–1331.
11. Roux KJ, Kim DI, Raida M, Burke B (2012) A promiscuous biotin ligase fusion protein identifies proximal and interacting proteins in mammalian cells. *J Cell Biol* 196(6):801–810.
12. To TL, et al. (2016) Photoactivatable protein labeling by singlet oxygen mediated reactions. *Bioorg Med Chem Lett* 26(14):3359–3363.
13. Moan J, Berg K (1991) The photodegradation of porphyrins in cells can be used to estimate the lifetime of singlet oxygen. *Photochem Photobiol* 53(4):549–553.
14. Baker A, Kanofsky JR (1992) Quenching of singlet oxygen by biomolecules from L1210 leukemia cells. *Photochem Photobiol* 55(4):523–528.
15. Silvester JA, Timmins GS, Davies MJ (1998) Protein hydroperoxides and carbonyl groups generated by porphyrin-induced photo-oxidation of bovine serum albumin. *Arch Biochem Biophys* 350(2):249–258.
16. Davies MJ (2004) Reactive species formed on proteins exposed to singlet oxygen. *Photochem Photobiol Sci* 3(1):17–25.
17. Nilsson R, Merkel PB, Kearns DR (1972) Unambiguous evidence for the participation of singlet oxygen (1) in photodynamic oxidation of amino acids. *Photochem Photobiol* 16(2):117–124.
18. Kim J, et al. (2008) Oxidative modification of cytochrome c by singlet oxygen. *Free Radic Biol Med* 44(9):1700–1711.
19. Davies MJ (2003) Singlet oxygen-mediated damage to proteins and its consequences. *Biochem Biophys Res Commun* 305(3):761–770.
20. Hensley K (2009) Detection of protein carbonyls by means of biotin hydrazide-streptavidin affinity methods. *Methods Mol Biol* 536:457–462.
21. Kalia J, Raines RT (2008) Hydrolytic stability of hydrazones and oximes. *Angew Chem Int Ed Engl* 47(39):7523–7526.
22. Wu AP, et al. (2011) Improved facial nerve identification with novel fluorescently labeled probe. *Laryngoscope* 121(4):805–810.
23. Hussain T, et al. (2015) Fluorescently labeled peptide increases identification of degenerated facial nerve branches during surgery and improves functional outcome. *PLoS One* 10(3):e0119600.
24. Timpl R, et al. (1979) Laminin–A glycoprotein from basement membranes. *J Biol Chem* 254(19):9933–9937.
25. Paulsson M, et al. (1987) Laminin-nidogen complex. Extraction with chelating agents and structural characterization. *Eur J Biochem* 166(1):11–19.
26. Chen P, Cescon M, Megighian A, Bonaldo P (2014) Collagen VI regulates peripheral nerve myelination and function. *FASEB J* 28(3):1145–1156.
27. Nareyeck G, et al. (2004) Differential interactions of decorin and decorin mutants with type I and type VI collagens. *Eur J Biochem* 271(16):3389–3398.
28. Patton BL, Miner JH, Chiu AY, Sanes JR (1997) Distribution and function of laminins in the neuromuscular system of developing, adult, and mutant mice. *J Cell Biol* 139(6):1507–1521.
29. von der Mark H, Aumailley M, Wick G, Fleischmajer R, Timpl R (1984) Immunochemistry, genuine size and tissue localization of collagen VI. *Eur J Biochem* 142(3):493–502.
30. Salonen V, Peltonen J, Röyttä M, Virtanen I (1987) Laminin in traumatized peripheral nerve: Basement membrane changes during degeneration and regeneration. *J Neurocytol* 16(5):713–720.
31. Wallquist W, et al. (2002) Laminin chains in rat and human peripheral nerve: Distribution and regulation during development and after axonal injury. *J Comp Neurol* 454(3):284–293.
32. Massaad CA, et al. (2015) Fluorescently-tagged anti-ganglioside antibody selectively identifies peripheral nerve in living animals. *Sci Rep* 5:15766.
33. Shu X, et al. (2011) A genetically encoded tag for correlated light and electron microscopy of intact cells, tissues, and organisms. *PLoS Biol* 9(4):e1001041.
34. Tour O, Meijer RM, Zacharias DA, Adams SR, Tsien RY (2003) Genetically targeted chromophore-assisted light inactivation. *Nat Biotechnol* 21(12):1505–1508.
35. To TL, Fadul MJ, Shu X (2014) Singlet oxygen triplet energy transfer-based imaging technology for mapping protein-protein proximity in intact cells. *Nat Commun* 5:4072.
36. Oien DB, et al. (2009) Detection of oxidized methionine in selected proteins, cellular extracts and blood serums by novel anti-methionine sulfoxide antibodies. *Arch Biochem Biophys* 485(1):35–40.
37. Ehrenshaft M, et al. (2009) Immunological detection of N-formylkynurenine in oxidized proteins. *Free Radic Biol Med* 46(9):1260–1266.
38. Shimoji Y, Ng V, Matsumura K, Fischetti VA, Rambukkana A (1999) A 21-kDa surface protein of Mycobacterium leprae binds peripheral nerve laminin-2 and mediates Schwann cell invasion. *Proc Natl Acad Sci USA* 96(17):9857–9862.
39. Ng V, et al. (2000) Role of the cell wall phenolic glycolipid-1 in the peripheral nerve predilection of Mycobacterium leprae. *Cell* 103(3):511–524.
40. Kessner D, Chambers M, Burke R, Agus D, Mallick P (2008) ProteoWizard: open source software for rapid proteomics tools development. *Bioinformatics* 24(21):2534–2536.
41. Eng JK, Jahan TA, Hoopmann MR (2013) Comet: an open-source MS/MS sequence database search tool. *Proteomics* 13(1):22–24.
42. Keller A, Nesvizhskii AI, Kolker E, Aebersold R (2002) Empirical statistical model to estimate the accuracy of peptide identifications made by MS/MS and database search. *Analytical chemistry* 74(20):5383–5392.
43. Choi M, et al. (2014) MSstats: an R package for statistical analysis of quantitative mass spectrometry-based proteomic experiments. *Bioinformatics* 30(17):2524–2526.

MEDICAL SCIENCES